Heliyon 7 (2021) e06056

Contents lists available at ScienceDirect

Heliyon

journal homepage: www.cell.com/heliyon

Research article

# Self-assembled nanostructures of L-ascorbic acid alkyl esters support monomeric amphotericin B

Natalia E. Nocelli [a,b], Yenisleidy de las Mercedes Zulueta Díaz [a,b], Marine Millot [a], María Luz Colazo [a], Raquel V. Vico [c,d], Maria Laura Fanani [a,b,*]

[a] Departamento de Química Biológica Ranwel Caputto, Facultad de Ciencias Químicas, Universidad Nacional de Córdoba, Córdoba, Argentina
[b] Centro de Investigaciones en Química Biológica de Córdoba (CIQUIBIC), CONICET, Córdoba, Argentina
[c] Departamento de Química Orgánica, Facultad de Ciencias Químicas, Universidad Nacional de Córdoba, Córdoba, Argentina
[d] Instituto de Investigaciones en Fisicoquímica de Córdoba (INFIQC-UNC–CONICET), Córdoba, Argentina

ARTICLE INFO

*Keywords:*
Amphiphilic drugs
Langmuir monolayers
Coagels
Polyene macrolides
Drug carriers

ABSTRACT

*Hypothesis:* Amphotericin B (AmB) is a highly effective antimicrobial, with broad antimycotic and antiparasitic effect. However, AmB poor water-solubilisation and aggregation tendency limits its use for topical applications. We studied the capacity of nanostructures formed by alkyl esters of L-ascorbic acid (ASCn) to solubilise AmB and tested the relationship between the prevalence of the monomeric form of AmB and its effectiveness as antimicrobial agent.

*Experiments:* We developed self-assembled nanostructures formed by the commercial compound, palmitoyl ascorbic acid, as well as the shorter chained myristoyl and lauroyl ascorbic acid. AmB loaded ASCn nanostructures were studied by a combination of spectroscopic techniques, together with particle analysis, differential scanning calorimetry, microbiological tests, and Langmuir monolayer visualisation.

*Findings:* We found no direct relation between the antimicrobial capacity and the prevalence of the monomeric form of the drug. However, the later was related to chemical stability and colloidal robustness. Nanostructures formed by ASC16 in its anionic state provide an appropriate environment for AmB in its monomeric form, maintaining its antimicrobial capacity. Langmuir film visualisation supports spectrophotometric evidence, indicating that ASC16 allows the in-plane solubilisation of AmB. Coagels formed by ASC16 appear as promising for carrying AmB for dermal delivery.

## 1. Introduction

Invasive fungal and parasitic infections are becoming a major health concern in various groups of patients leading to severe morbidity and mortality. Despite the availability of effective agents in the antifungal and antiparasitic drug treatments, their therapeutic outcome is less than optimal due to limitations related to the drugs' physicochemical properties [1] and in many cases, due to their high economic costs.

Amphotericin B (AmB) is a potent antimicrobial agent [2] and is the drug of choice for life-threatening systemic infections with fungi. However, no commercial form of AmB for topical administration is currently available. AmB is used as a second-line treatment for cutaneous Leishmaniasis [3,4], highlighted by the World Health Organization as one of the so-called neglected diseases with high incidence in tropical and subtropical regions, such as South America. However, for the treatment of this cutaneous disease, AmB is administered in a parenteral form, causing toxic side effects. The invasiveness of the standard treatment protocol means that many patients fail to complete their full course of treatment. Hence, to reduce systemic toxic effects, economic cost, and poor treatment compliance, research has focused on the development of alternative dosage schedules and topical treatments [4].

AmB has also been proved to be highly efficient against cutaneous candidiasis. However, its use is limited due to skin irritation [5]. Ointments are not recommended for treating this cutaneous disease, because of their potential for entrapping excessive moisture [6], and therefore water-based formulations with high antifungal efficiency are desirable for its treatment, in particular, in cases resistant to conventional antifungal drugs. Several attempts have been made to achieve an effective

* Corresponding author.
*E-mail address:* lfanani@fcq.unc.edu.ar (M.L. Fanani).

https://doi.org/10.1016/j.heliyon.2021.e06056
Received 4 May 2020; Received in revised form 3 November 2020; Accepted 19 January 2021

topical formulation for AmB dermal or transdermal delivery. The strategies employed usually involve encapsulation in cyclodextrin, liposomal or colloidal systems [1,7–11].

AmB is an amphiphilic molecule with a hydrophobic side composed of polyene and a hydrophilic side composed of multiple hydroxyl groups [12] (Scheme 1). Its structure contains a carboxylic acid and an amino group with $pK_a$ of 5.7 and 10, respectively. Therefore, at physiological pH, both the acid and the amino group are ionised, whilst at pH 4 it is in its cationic form.

Several works report that its mechanism of action involves drug molecule concentration in cell membranes [12]. The presence of sterols promotes a change in the orientation of AmB molecules from parallel to perpendicular to the membrane surface, penetrating the membrane [13]. Once incorporated into cell membranes, AmB forms channel-like structures (formed by two half pores) spanning the lipid bilayer [12]. It has also been reported that ergosterol (a characteristic fungal sterol) facilitates the association of AmB dimers into aggregates destabilising the membrane, whilst cholesterol inhibits this [13].

Due to the lipophilic nature of AmB, the drug tends to aggregate in aqueous solution, resulting in low water solubility [14]. Pioneer works in the early 90s established a relationship between oligomeric state of AmB and its interaction with sterol-enriched membranes [15], erythrocytes and yeast cells [16,17] and its toxicity in mice [18]. Therefore, a search for new less toxic AmB formulation was focused on achieving a formulation capable to keep the drug in its monomeric form, as detected by UV-visible and circular dichroism (CD) spectroscopy. Nowadays, it is widely accepted that the toxicity of AmB is in some way mediated by the aggregated forms of the drug [1,14,16,17,19]. In turn, the self-association behaviour of AmB depends on the local environment [20]. Monomers, as well as soluble and insoluble self-associated AmB, are present in the aqueous solution above ~0.2 μg/mL (~0.2 μM). Additionally, the oxidant power of AmB induces oxidative damage and toxicity [21]. Therefore, although AmB is highly effective, these problems present important clinical limitations for its use.

Surfactants increase AmB solubility in water. This is the case of sodium deoxycholate, present in the commercial form of AmB: Fungizone®

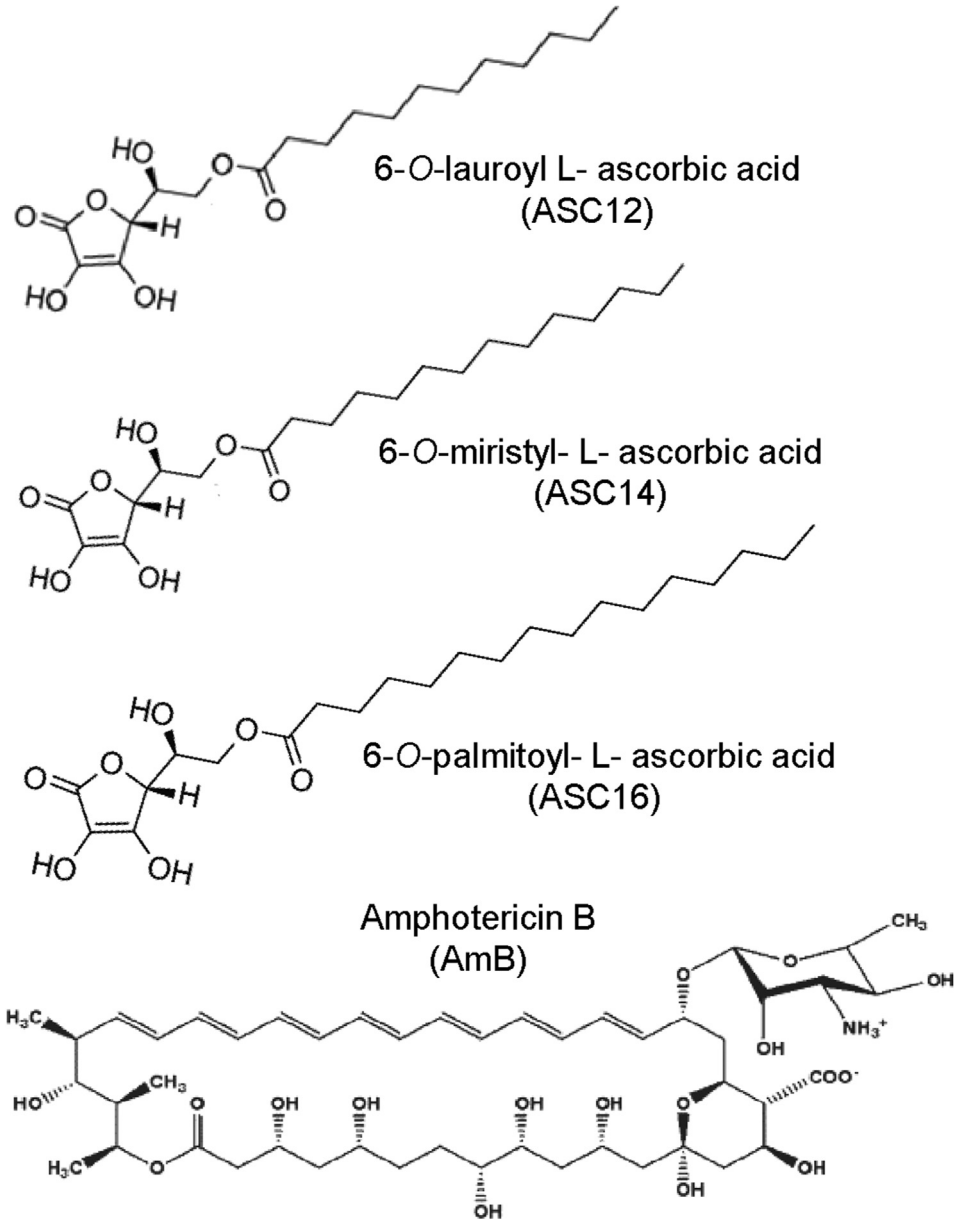


**Scheme 1.** Chemical structure of amphiphilic compounds used in the present work. Source: pubchem.ncbi.nlm.nih.gov.

(Bristol Myers-Squibb, Princeton, NJ), a freeze-dried powder, which on reconstitution yields a micellar solution of AmB. However, this formulation is still associated with side effects such as fever and chills, nausea, haemolysis and considerable nephrotoxicity [2].

AmB can be considered as the drug model for testing drug targeting. Many drug-carrier systems have been loaded and tested with AmB [2, 22]. The severe side effects of AmB have been partially overcome by lipid-based formulations, such as Ambisome (Liposomal Amphotericin B), Abelcet (dispersion of ribbon-like AmB - lipid complex) and Amphocil (colloidal dispersion of AmB - cholesteryl sulphate complex), [1,23]. However, lipid-based AmB use is still limited to some extent by adverse effects. In addition, their high cost for treatment restricts their use.

Heat treatment has been employed to reach super-aggregated forms of AmB with particular spectroscopic characteristics and with improved tolerance in clinical use [24]. Several studies also report that micellar [25–27] and nanostructured [1,28,29] AmB suspensions have been successful in maintaining the monomeric form of AmB and are promising as therapeutic formulations with putative low side effects. The results obtained using micellar formulations of polymers [26,30] and the natural glycolipid GM1 [25] are particularly interesting.

L-ascorbic acid alkyl esters (ASCn) are lipophilic forms of vitamin C (Scheme 1) with pharmacological interest due to their antioxidant properties and amphiphilic behaviour [31,32]. The presence of the acyl chain improves their solubility in alcohol and non-polar solvents and provides them with the capacity to self-organise into micelles and liquid crystal forms called coagels, when they are dispersed in water [31,33]. The surface activity and self-organisation properties of ASCn strongly depend on their ionisation form and electrostatic conditions as well as the length of their acyl chain [33,34]. The versatility of their aggregation properties and their chemical stability [34] make them a promising tool as drug carriers in pharmaceutical formulations [35–37] as well as in new adjuvant preparations [38] and liposome-based drug delivery systems [39]. Dermal and ocular delivery of drugs has been previously investigated to be effective by using ASCn coagel containing 2–5 % w/w as drug carriers and permeation enhancers [35,36,40]. Therefore, the study of concentrated ASCn suspensions is relevant in the context of the potential use of the coagels in the topical treatment of infectious diseases.

Here, we studied the capacity of the nanostructures formed by ASCn to solubilise AmB for effective antimitotic activity, using biotechnology to respond to society's demand for new solutions to the problems related to cutaneous leishmaniasis as well to other diseases such as cutaneous candidiasis. We developed self-assembled nanostructures formed by the commercial compound, palmitoyl ascorbic acid (ASC16), as well as the shorter chained myristoyl (ASC14) and lauroyl ascorbic acid (ASC12), synthesised in our laboratory. ASCn have low CMC (micromolar) and ASC16 is an approved excipient for use in humans. The high antioxidant power provided by the ascorbyl moiety of ASCn, in addition to their capacity to self-aggregate into lamellar water-soluble nanostructures [34], offer notable advantages over oil-based and cream formulations for cutaneous treatment. Considering that ASCn are also proposed as skin permeation enhancers [41] and are synthesised easily and at low-cost [42], the ASCn family is appealing as AmB carriers for topical AmB administration.

A combination of spectroscopic and physicochemical studies is presented in this work, together with particle analysis, differential scanning calorimetry and Langmuir monolayer visualisation. Combined with microbiological tests, these studies encourage further tests of ASC16 coagels, for carrying AmB dermal delivery. Our results advance the understanding of the capacity of ASCn to support the monomeric AmB, based on their electrostatic and thermodynamic properties as well as the in-plane structure of the ASCn supramolecular arrangements.

## 2. Materials and methods

### 2.1. Materials

Commercial 6-*O*-Palmitoyl-L-ascorbic acid (ASC16) was supplied by Sigma-Aldrich and exhaustively purified as described in Ref. [34]. 6-*O*-Myristic-L-ascorbic acid (ASC14) and 6-*O*-Lauric-L-ascorbic acid (ASC12) were synthesised and purified as described in Ref. [34]. Amphotericin B (AmB), analytical standard quality, was also purchased from Sigma Aldrich. All other reagents were of analytical grade (99% pure) and used without further purification. The water was purified by a Milli-Q (Millipore, Billerica, MA USA) system, to yield a product with a resistivity of ~18.5 MΩ cm.

### 2.2. Preparation of ASCn formulations

Coagels were prepared by mixing the components (from an ethanol stock solution of ASCn and AmB in DMSO) in appropriate proportions in microtubes. The solvent evaporation was performed by using a vacuum concentrator treatment (SpeedVac, Thermo Fisher Scientific) for 5 h. The dry drugs were hydrated in 5 mM Tris-HCl, pH 8 or 5 mM citrate buffer pH 4 to reach a final concentration of 2% w/v of ASCn and 0.1% w/v of AmB (1.02 mM), and an ASCn/AmB ratio of 20 (w/w). The dispersions were heated to 65 °C (above the critical micellar temperature, CMT of all ASCn) [28] followed by stirring and the temperature was decreased to 0 °C, repeating these steps in three cycles, then homogenised in an ultrasound bath for 15 min and allowed to reach room temperature in closed tubes. It has been reported that the treatment of AmB at 65 °C does not alter molecular stability or therapeutic properties [20]. DSC experiments were performed using coagel preparation. Spectroscopic studies as well as particle analysis were performed by dispersing the coagels in a 1/50 dilution (unless specified) in 5 mM Tris-HCl, pH 8, or 5 mM citrate buffer pH 4. In this diluted dispersion, AmB concentration was 20.4 μM.

### 2.3. Amphotericin B (AmB) monomer/aggregate evaluation

AmB UV-visible absorption spectra of the diluted preparations were acquired at 300–450 nm (0.5 nm steps, slits 0.5) in a Shimadzu UV-2401PC and using a 3 mm quartz cell at room temperature. The aggregation state of encapsulated AmB was assessed by the ratio of the first aand last peak (I/IV) in the absorbance spectra [19]. Circular dichroism (CD) spectra were acquired in a Jasco J-810 spectropolarimeter. The CD spectra were recorded (300–450 nm) by using a 10 mm quartz cell at room temperature. The setup parameters used were resolution 0.5 nm, bandwidth 4 nm, sensitivity 2 s, and scan speed 100 nm/min. Three scans were acquired and averaged for each sample. Raw data were manipulated by subtraction of the appropriate background spectra containing the corresponding ASCn in the buffer at pH 4 or pH 8.

### 2.4. Particle analysis

The size-distribution of particles of diluted suspension of ASCn/AmB (1/50 dilution) was studied by dynamic light scattering (DLS) using a 530 nm laser beam and the scattered light was analysed at 90° through the adjustment of a correlation function. The hydrodynamic diameter of the particles was determined by the Stokes-Einstein equation. The equipment used was a Submicron Particle Sizer, NicompTM 380, Santa Barbara, California, USA). Zeta potential measurements were performed using the Zsizer SZ-100Z equipment (Horiba, Ltd., Japan), provided with a semiconductor laser excitation solid-state laser (532 nm, 10 mW) and using the laser-Doppler velocimetry technique. For both tests, the samples were degassed by vacuum treatment for 10 min before analysis. The experiments were conducted at 22 ± 1 °C.

Sedimentation experiments were performed by centrifugation of diluted suspension of ASCn/AmB (1/50 dilution) at different speeds

(800–3000 rpm). 20 μL of the supernatant was collected after each centrifugation cycle (10 min) and 80 μL of ethanol (95%) was added before spectroscopic analysis. AmB content was calculated from the absorbance at 407 nm and ASC12 and ASC16 from the absorbance at 250 and 267 nm, respectively. In these conditions, ASCn absorbance was linear with concentration up to 200 μM.

### 2.5. Differential scanning calorimetry (DSC) measurements

ASC16 and ASC12 coagels were analysed by DSC. The samples, before being loading into a Microcal VP-DSC Scanning Calorimeter (Microcal, Northampton, MA, USA), were subjected to 15 min of vacuum treatment. The appropriate buffer was used in the reference cell. Thermograms were recorded over a temperature range from 20 to 85 °C, at a heating rate of 30 °C/h and analysed with Microcal Origin 8.0 software (Microcal, Northampton, MA, USA). Baselines were created and subtracted from the thermograms and the plots were normalised according to the total amphiphilic concentration.

### 2.6. Inhibition of yeast growth by diffusion test of ASC16/AmB coagels

The diffusion of AmB from ASC16 coagels and antimicrobial activity was tested by the agar surfacediffusion method, a variant of the diffusion well method. Briefly, the sample to be tested is placed onto the surface of an inoculated medium and, after incubation, the diameter of the clear zone around the reservoir (inhibition halo) is measured [43]. The yeast strain used was *Saccharomyces cerevisiae* BY4741, ATCC 201388 [44], which was cultivated in sterile yeasts peptone dextrose (YPD) culture medium, at pH 6.5, 30 °C, 24 h and under continuous agitation at 150 rpm. The number of viable cells was determined by using the micro-droplet technique [45]. It consisted of performing serial dilutions of the culture and sowing on Petri dishes containing sterile solid medium (YPD). The dishes were incubated at 30 °C during 24 h and the colonies were counted. For the antimicrobial test of coagel preparations, agar plates were seeded with sterile swabs, achieving confluent growth containing about $5 \times 10^6$ cfu $mL^{-1}$ over the entire surface. On the already seeded surface, drops of 20 μL of each coagel to be evaluated, containing 2 μg of AmB, and their respective controls were placed in triplicate, and allowed to rest for 30 min ASC16/AmB formulation (pH 8) with a ratio (w/w) of 5, 10, 15 and 20 were tested. Aqueous suspension of AmB at pH4 or 8, as well as ASC16 or ASC12 coagles in the absence of AmB were also tested. Finally, the Petri dishes were incubated at 30 ± 2 °C for 24 the inhibition halos were subsequently measured.

### 2.7. Brewster Angle Microscopy of Langmuir films

Amphiphile monolayers were prepared and characterised in a Langmuir film balance with uniaxial compression, as detailed before [46], onto a Tris-HCl 5 mM (pH 8) or Citrate 5 mM (pH 4) subphase at 23 ± 1 °C. The surface pressure was determined using the Wilhelmy method with a Pt plate according to Eq. (1),

$$\pi = \gamma_0 - \gamma \qquad \text{(eq. 1)}$$

where $\gamma_0$ and $\gamma$ denote the surface tension respectively before and after amphiphile spreading at the interface. After solvent evaporation and relaxation at $\pi \leq 0.5$ mN/m (~5 min), the film was compressed at a rate of 2.0 ± 0.5 $Å^2.molec^{-1}.min^{-1}$, until reaching collapse pressure by reducing the area between two Delrin™ barriers. Their lateral movement over the trough surface was controlled and registered by an electronic unit.

The monolayers were observed while compressed, using a KSV–NIMA *Langmuir minitrough* (Helsinki, Finland) mounted on the stage of a Nanofilm EP3 Imaging Ellipsometer (Accurion, Göttingen, Germany), which was used in the Brewster Angle Microscopy (BAM) mode. Zero reflection was set with a polarised laser ($\lambda = 532$ nm) incident on the bare aqueous surface at the experimentally calibrated Brewster angle (≈53.1°). After monolayer formation and compression, the reflected light was collected with a 20 × objective.

The grey level of each pixel of the BAM images corresponds to reflectivity values after calibration factors tested for each experiment. The reflectivity ($R_p$) is in turn related to film thickness and the refraction index of the film ($l$), according to the following equation [47].

$$l = \frac{\sqrt{R_p}}{\sin(2\theta_B - 90)} \cdot \frac{\lambda}{\pi} \cdot \frac{\left(n_1^2 - n_2^2\right)}{\sqrt{n_1^2 + n_2^2}} \cdot \frac{n^2}{(n_1^2 - n^2)(n_2^2 - n^2)} \qquad \text{(eq. 2)}$$

where $n_1$ is the refractive index of the air ($n_1 = 1$), $n_2$ is the refractive index of the subphase (1.33) and $\lambda$ is the laser wavelength (523 nm). $n$ is the refractive index of the film, which was assumed to be 1.440 for compact films or 1.433 for expanded films [48]. Average reflectivity was calculated from the grey level of each image, measured by using the free software ImageJ 1.43u (NIH, USA) and calculated after the calibration parameters.

### 2.8. Statistical analysis

The assays were performed in triplicate and repeated three times. The data were subjected to a one-way analysis of variance (ANOVA), followed by a comparison of multiple treatment levels with the control by using Tukey's least significant difference *post hoc* test. In this system, two populations will be labelled with the same capital letter if the statistical discrepancies between both conditions are smaller than p-value = 0.05. All statistical analyses were performed using the free software InfoStat (Di Rienzo J.A., Casanoves F., Balzarini M.G., Gonzalez L., Tablada M., Robledo C.W. InfoStat version 2019. Centro de Transferencia InfoStat, FCA, Universidad Nacional de Córdoba, Argentina. URL http://www.infostat.com.ar).

## 3. Results

### 3.1. ASCn aqueous dispersion supports monomeric and oligomeric AmB depending on electrostatic properties and the acyl chain length of the derivative

Vitamin C amphiphilic derivatives were used, substituted by acyl chains (ASCn) of three different lengths (C16, C14, and C12) forming ascorbyl palmitate (ASC16), ascorbyl myristate (ASC14) and ascorbyl laurate (ASC12), respectively. ASCn have been studied dispersed in a buffer solution at pH 8, where the molecules are mainly in an anionic form (the $C_3$–OH group of the ascorbic moiety have a $pK_a$ of 4.2) and at pH 4. At pH 4, the compounds are mainly neutral as a consequence of an ion double layer effect induced by the lamellar structure of the ASCn aggregates (see Figure S1 and S2A in supplementary information file and Ref. [46]). The (ionised) ascorbic moieties self-organise in a plane and attract $H^+$ to the interface, lowering the surface pH to an extent that depends on the ionic strength. Therefore, when the bulk pH is 4, the surface pH falls to ~3 in the presence of 145 mM NaCl, and the dissociation fraction is expected to be ~10% in the presence of salt [46].

Coagels of ASCn 2% (w/v) were formed with the addition of 0.1% (w/v) of AmB, obtaining a preparation with an ASCn/AmB ratio of 20 (w/w). These preparations were directly analysed by differential scanning calorimetry (DSC) (see section 3.2) and antimicrobial activity (see section 3.3). For absorption spectroscopy and nanoparticle analysis, coagels were diluted 1/50 fold in their respective buffer solutions.

The relative aggregation state of AmB was assessed by UV-visible absorption and CD spectroscopy. ASCn show a strong absorption band centred at 248–268 nm, depending on the acyl chain length and the pH of the buffer media (not shown). Since ASCn are 20 folds more concentrated than AmB in the formulation studied, and the work was focused on AmB, for the sack of simplicity in Figure 1 we only show spectra in the 300–450 nm range. The typical absorption spectrum of AmB in its monomeric form

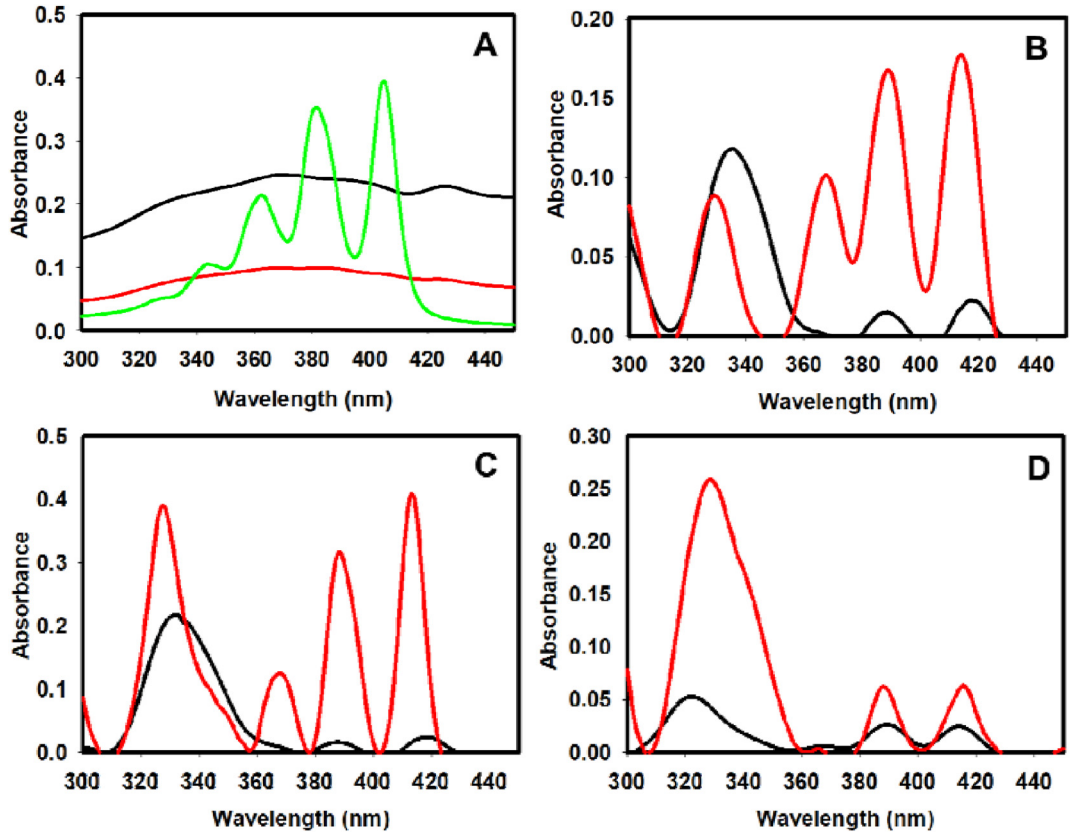


**Figure 1.** UV-visible absorption spectra of pure AmB and alkyl esters of L-Ascorbic Acid (ASCn)/AmB formulation at two different pH. The spectra correspond to (A) AmB in methanol (green line) or in buffer solution at pH4 or pH8; C-D) AmB with ASCn in aqueous suspension: ascorbyl palmitate (ASC16) (B), ascorbyl myristate (ASC14) (C) and ascorbyl laurate (ASC12) (D) formulations. AmB concentration was 20.4 μM. Aqueous suspensions are at pH 4 (black lines) and pH8 (red lines). The spectra are the average of three independent experiments.

contains four primary peaks centred at 344, 364, 382 and 405 nm, as can be observed in the methanol solution spectrum (Figure 1A and Table S1 in Supplementary Material). AmB in aqueous solution present flattened absorption spectra, with poorly defined peaks both at pH4 and pH 8. The suspension of AmB in an aqueous environment changes the relative height of the peaks giving importance to the first band (I), which corresponds to a self-aggregated (oligomeric) form. Hypsochromic and bathochromic shifts in the electronic absorption spectrum has been also associated with the aggregation processes of antibiotic molecules [49, 50]. Figure 1B-D as well as Table S1 shows the hypsochromic shift of peak I and bathochromic shift of peak IV, for ASCn/AmB formulations in comparison with AmB in methanol. The ratio of the and the last peak (I/IV) in the absorbance spectrum gives low values in methanol solutions (0.4, see Figure 2) compared with the reported peak ratio (I/IV) for aqueous suspension of AmB at pH 4 and 8 (values close to 1, see Figure 1A and Ref. [51]).

The UV-visible absorption spectra of the ASCn/AmB diluted preparations (AmB concentration 20.4 μM and ASCn 960 μM) show different profiles depending on the acyl chain length of the ASCn and the electrostatic condition of the samples. All three formulations of ASCn/AmB formed at pH4 show the preponderance of the first band in the absorption spectra (Figure 1) and I/IV ratios $\geq$2 (Figure 2). Additionally, a bathochromic shift of the IV band (see Table S1) suggest the formation of J-aggregates, where AmB molecules primarily stack in a head-to-tail arrangement [50].

On the other hand, the formulations of ASCn/AmB in pH conditions, where the ascorbic derivatives are present in anionic form (pH 8), show the increasing contribution of the monomeric AmB peaks and a lowering of the I/IV ratio, with the increasing length of the ASCn acyl chains (Figure 2). The spectra evidence coexistence of monomeric and

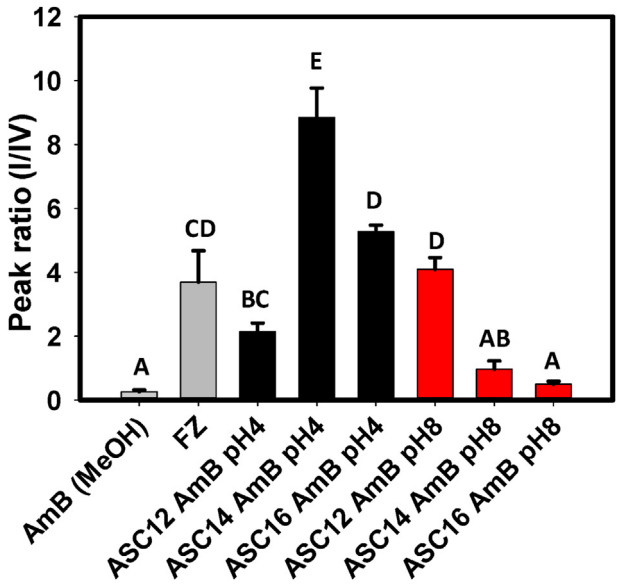


**Figure 2.** Ratio of maxima absorbance intensity of peaks I/IV of UV-visible absorbance spectrum of AmB in an organic solvent (methanol), commercial formulation Fungazone® (FZ, taken from Ref. [52]) or the ASCn/AmB formulation at pH4 (grey bars) or pH8 (red bars). ASCn/AmB formulations are as described in Figure 1. Error bars are SD from three independent experiments. Different capital letters indicate statistical discrepancies between conditions according to Tukey's least significant difference test ($p < 0.05$), see section 2.7.

oligomeric forms of AmB. The hypsochromic shift of the band I, which is more pronounced for ASC16 and ASC14 formulations at pH 4 (Table S1), is connected with the forming of H-type aggregated molecular structures (where molecules stack predominantly face-to-face), where the transition dipole moments of molecules are orientated parallel and the out of the plane of aggregate [50]. Notably, the ASC16/AmB formulation at pH8 shows a I/IV ratio of 0.6, which is comparable with that reported for AmB solubilised in GM1 micelles [25] and copolymers [26,30]. In our study, the I/V ratio for ASC16/AmB suspension at pH 8 is not statistically different than that obtained for AmB solubilised in methanol.

To confirm the aggregation state of AmB in the different ASCn formulations, we performed circular dichroism (CD) experiments (Figure 3). It is well known that CD spectra of AmB in aqueous media are concentration-dependent. At above 100 μM, AmB exists in a highly aggregated form, while in the (0.1–1) μM range it is believed to coexist as a mixture of dimers and higher-order assemblies. In the aggregated form, the CD spectra of AmB show an asymmetric doublet centred at about 340 nm, while the monomeric form in aqueous solution (concentrations less than 0.1 μM) is undetectable by CD spectroscopy [14,53–55].

The ASCn/AmB formulations at both pHs show CD profiles in line with the aggregation state observed by UV-visible spectroscopy, confirming these results. The CD spectra reveal the main contribution of the aggregated form for all ASCn at pH 4 being ASC12 > ASC14 > ASC16. When ASCn is in the anionic state (pH 8), ASC14 and ASC12 support AmB mainly in the aggregated form. Interestingly, the CD spectrum of ASC16/AmB at pH 8 reveals the coexistence of the aggregated and monomeric forms of the drug, thus confirming the occurrence of monomeric AmB in this formulation. Clearly, the monomer concentration in ASC16/AmB at pH 8 is considerably higher and could be detected by means of CD spectroscopy in the aqueous medium (see inset in Figure 3A).

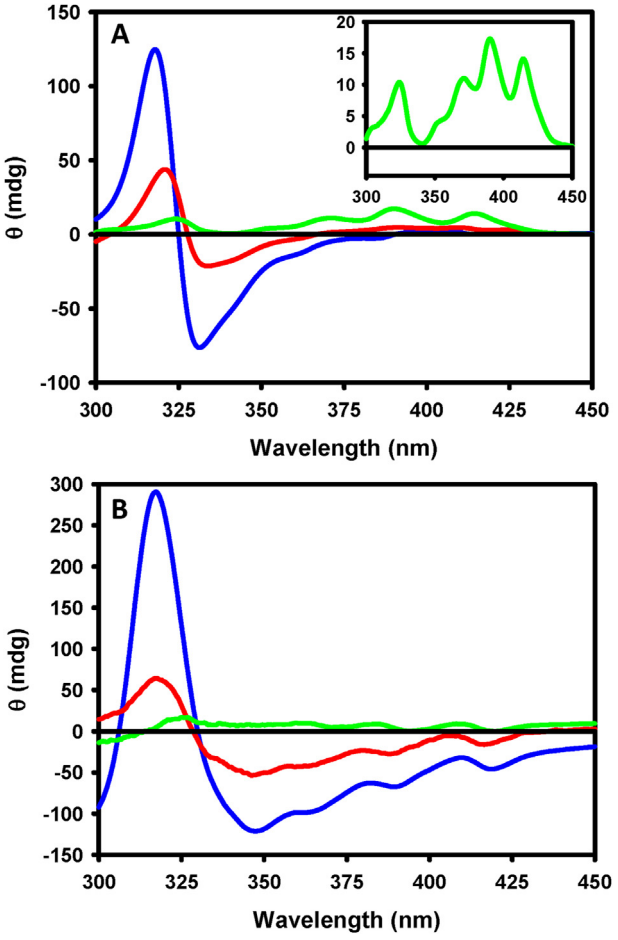


**Figure 3.** Circular dichroism spectra of alkyl esters of L-Ascorbic Acid (ASCn)/AmB formulation at pH 8 (A) or pH 4 (B). The spectra correspond to AmB with ASCn in aqueous suspension: ascorbyl palmitate (ASC16) (green), ascorbyl myristate (ASC14) (red) and ascorbyl laurate (ASC12) (blue) formulations. AmB concentration was 20.4 μM. The inset in A shows an amplified section of ASC16/AmB spectrum.

Based on the above data, the ASC16/AmB formulation at pH 8 was taken as the most promising formulation capable of sustaining AmB in its monomeric form and, therefore, having the potentiality of being a more effective antimicrobial formulation. On the contrary, ASC12/AmB at pH 4 appears as the formulation with less capacity for maintaining AmB in the monomeric form. We next explored the hypothesis that the monomeric/aggregate ratio of AmB in the nanoformulation will determine its antimicrobial effectivity.

### 3.2. Antimicrobial activity and stability of ASC16/AmB and ASC12/AmB coagels

We choose to performed antimicrobial capacity tests for the ASC16/AmB and ASC12/AmB formulation by the agar surface diffusion method, a variant of the agar well diffusion method. ASC16 coagels formed at pH8 without the addition of AmB showed no antimicrobial capacity, whilst ASC12 coagels at pH4 showed a limited antimicrobial activity (Figure 4). AmB inclusion into ASC16 coagel at pH8 did not alter its antimicrobial activity for all the formulation studied, containing different ASC16/AmB (w/w) ratio. On the contrary, the incorporation of AmB on ASC12 coagels at pH4 improves the antimicrobial activity of AmB in a significant amount (Figure 4). This unexpected enhancement of antifungal activity for the ASC12/AmB (pH4) formulation may be a consequence of combined effect of AmB and ASC12. Notably, those results do not agree with previous observations regarding the greater effectiveness of the AmB monomeric form in comparison with the aggregated forms. On the other hand, as the microbiological test performed is affected by the diffusion properties of the suspension components as well as AmB antimicrobial effectivity, this enhancement effect observed for ASC12/AmB may be related to these diffusional aspects.

The ASCn/AmB formulation used for this test were explored by absorption spectroscopy. Figure S3 shows that a decrease in the ASC16 content in the formulation increases the band I/IV ratio of AmB absorption spectrum, evidencing AmB oligomerization. This highlights the finding that formulation with different spectroscopic behaviour shows similar antimicrobial activity (Figure 4). On the other hand, ASC12/AmB suspension spectrum kept similar characteristics against a decrease in the ASC12/AmB ratio.

We further studied the robustness of the capacity of ASCn/AmB formulations to maintain AmB in its monomeric form with dilution. The data shown in Figure S4 indicates that ASC16/AmB coagel (pH8) dilutions from 1/10 to 1/50, sustains AmB mainly in its monomeric form. This provides evidence of a stable inclusion of AmB in the ASC16 coagel, a property relevant for its proposed therapeutically usage.

The concept of monomeric AmB being more efficient antimicrobials than aggregated AmB was established in the 90s through studies on model lipid membranes containing cholesterol or ergosterol [15]. Further studies on the toxicity of the soluble and/or aggregated forms of AmB followed those works [16,18,21]. However, in those studies, activity and toxicity results are confused and mixed together. On the other hand, those observed effects may be influenced by different chemical stability as well as colloidal stability of the AmB suspensions. The difference in literature and our results may arise from the difficulty to compare AmB antimicrobial activity from formulations that share similar physicochemical characteristics (such as water-soluble, colloidal suspension, etc.) and show different monomeric/oligomeric AmB forms. In the present work, we have the opportunity to compare two water-soluble, colloidal formulations of similar characteristics with different prevalence of monomeric or oligomeric forms of AmB. We will correlate its antimicrobial effect and its chemical and particle stability through spectroscopic and particle analysis studies.

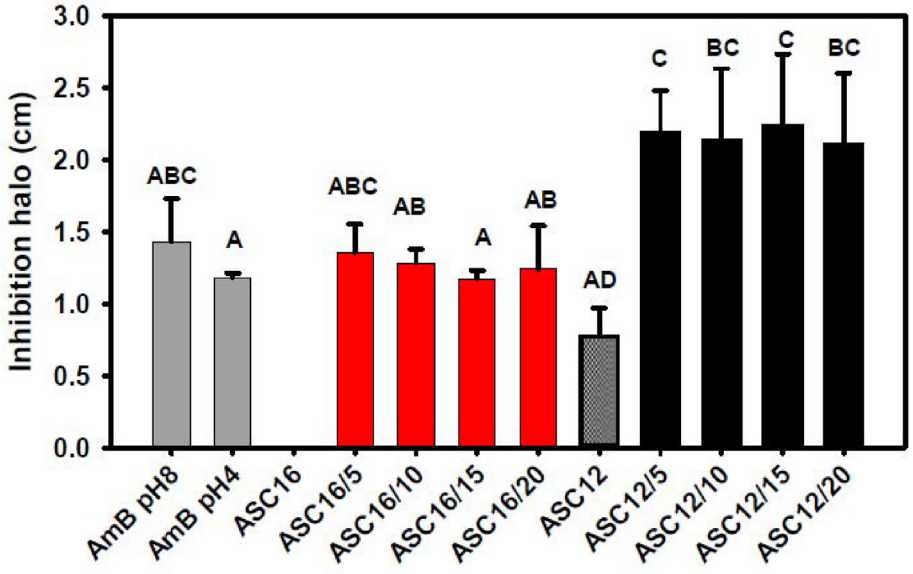


**Figure 4.** Inhibition of growth of *Saccharomyces cerevisiae* BY4741 assessed by the agar surface diffusion method. The samples contained AmB in buffer solution at pH4 or 8 and ASC16 (pH8) and ASC12 (pH4) coagels in the absence or presence of AmB. ASCn/AmB ratio (w/w) was of 0, 5, 10, 15 and 20. All the sampes assayed contained 2 μg of AmB, with the exception of the pure ASC16 or ASC12 control. The data is the mean value of three independent tests performed in triplicate and the error bar corresponds to SD. Different capital letters indicate statistic discrepancies between conditions according to the test of Tukey's least significant difference test ($P < 0.05$), see section 2.8.

Chemical stability studies of AmB in ASC16/AmB formulation (pH 8) were conducted for two weeks, stored in the dark and at room temperature. Figure 5A shows that their absorption spectra retain the characteristic profile of the monomeric form of AmB (I/IV ratio 0.4 at 15 days post preparation). Some changes in the peaks intensity are evident after several incubation days. The increase of the peak ratio III/IV has been proposed as a consequence of polyene oxidation [56], and an increase in peak I also suggest a moderate increase in the aggregation state of AmB over time. As will be discussed in section 3.3, the supramolecular structure formed by ASC16 at pH8 shows the coexistence of a micellar and a lamellar phase. Those structures undergo annealing with the preponderance of the micellar phase over an extended amount of time. Those structures may provide slightly different environments for the AmB molecules that result in the changes in the spectroscopy properties observed in Figure 5.

In contrast, the ASC12/AmB formulation at pH 4 (Figure 5B) showed an absorbance spectrum characteristic of AmB aggregates during the first week of storage, with an increase of the intensity of peak I and a bathochromic shift of peak IV, suggesting J-aggregates formation [50]. A loss in absorbance intensity at longer times (two weeks) suggests further degradation of the drug or loss due to precipitation. This effect may be related to the lower chemical stability of AmB observed in aqueous solutions in acidic conditions [2].

Sedimentation studies were performed to assess the stability of the colloidal suspensions. Diluted coagels (1/50) were subjected to centrifugation at crescent speed and the content of AmB and ASCn in the supernatant was analysed spectrophotometrically. Full sedimentation of the particles (not spectroscopic signals observed) was reached at 3000 rpm for ASC16/AmB suspension and at 2000 rpm for ASC12/AmB samples (not shown), evidencing larger robustness of the ASC16 (pH8) colloidal suspension. In order to study if AmB molecules were mainly integrated into ASC16 or ASC12 self-assembled structures or formed separated aggregates, the ratio of ASCn/AmB peak intensity was analysed. If AmB-enriched particles were present, a different sedimentation speed would be observed than the ASCn particles.

Figure S5 shows that the ratio of ASC16/AmB peak intensity was relatively constant along the centrifugation speed conditions studied. The ASC12/AmB system show a slight tendency to increase the ASC12/AmB peak ratio observed in the supernatant but showing large dispersion of the data. This suggests a larger heterogeneity in the behaviour of the particles but supporting that AmB would be integrated into the ASC12

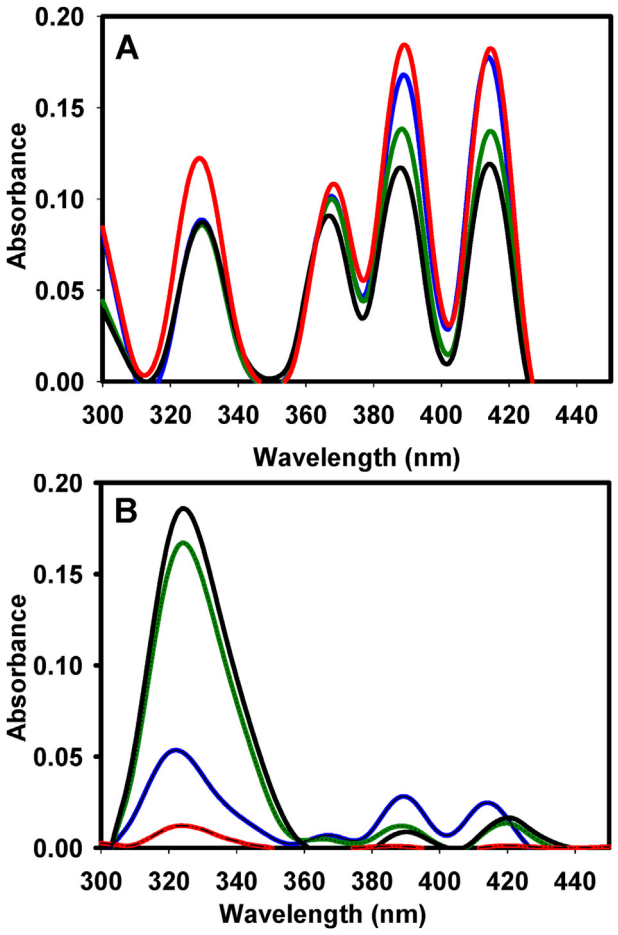


**Figure 5.** Time Stability of ASCn/AmB formulation. Absorption spectra at day 0 (blue line), 3 (green line), 7 (black line) and 15 (red line) after producing ASC16/AmB at pH 8 (A) or ASC12/AmB at pH 4 (B) and stored in the dark at room temperature. Final AmB concentration 20.4 μM. The spectra are the average of three independent experiments.

structures and not forming segregated particles, which could sediment independently.

The results discussed above indicate that even when AmB is active against yeast cells when incorporated into the ASC12 (pH4) or the ASC16 (pH8) coagels, both the chemical and colloidal stability of the first formulation are lower in comparison with the one containing ASC16. Integrating those results and the spectroscopic studies presented in section 3.1, we can conclude that the effective antimicrobial activity expected for AmB in topical applications may be more related to the suspension stability and AmB chemical protection than to the actual monomer/oligomer forms ratio. Further studies on the physicochemical characteristics of the ASCn/AmB suspensions were performed to advance on the perspective of those formulations for therapeutic usage.

### 3.3. Physicochemical characterisation of ASCn/AmB formulations

ASCn aqueous suspensions show critical monomer concentrations (CMC) in equilibrium with the aggregated forms in the 8–35 μM concentration range, depending on the length of the acyl chain [34]. Above this concentration range, ASC16 form liquid crystals with a lamellar structure, as detected by the X-scattering technique [33]. However, the presence of a new component, such as AmB, can affect the self-organisation properties of ASCn, altering the equilibrium between different particle populations. In the present section, we characterise the self-assembly particles formed by ASCn/AmB. The inspection of ASCn/AmB diluted preparations (1/50-fold dilution of coagels) shows the presence of nano-as well as micro-size particles, as inspected by dynamic light scattering (DLS) (Figure 6).

For ASCn/AmB suspensions formed at pH 8, micelle-size particles (10–30 nm diameter) as well as other small nanostructures (50–100 nm) occurred, whilst at pH 4, micrometer-sized particles were mainly observed. This behaviour can be explained by the differences in the electrostatic properties of the ASCn aggregates. At pH 4, when ASCn are below their $pK_a$ (4.2), the particles show negative values of zeta potential in the (-15) to (-25) mV range (Figure S1, in the supplementary information file). On the other hand, at pH > $pK_a$ (pH 8), a high degree of ionisation is expected for ASCn and the zeta potential values drop to (-60 - -80) mV. This high degree of ionisation implies high lateral intermolecular repulsion among the particle components and favours the occurrence of smaller, more relaxed structures such as micelles or small vesicles. This correlates with previous observations of ASCn forming more expanded Langmuir films at neutral pH in comparison with acidic pH (see Figure S2 and Ref. [33,34,46]).

ASCn suspensions in absence of AmB show similar particle size distribution patterns (not shown), indicating that, at the proportion used (ASCn/AmB = 20), the zwitterionic character of AmB does not influence the electrostatic properties of the nanostructures, at least in the nanoscale, and the ASCn components dominate the self-assembly structuring.

The thermal behaviour of ASCn coagels has been previously studied and melting temperatures of 47.3, 56.0, and 63.8 °C were reported for ASC12, ASC14, and ASC16, respectively [32]. However, the samples assayed were prepared in pure water. On the other hand, ascorbyl palmitate sodium salt was reported to show a melting point of 26 °C [57]. Previous studies by our group have shown a strong ion double-layer effect on the behaviour of ASCn monolayer and aqueous suspensions [33, 34,46]. In those works, the supramolecular structure of the self-assembled systems matches an effective pH (at the amphiphile/aqueous interface) two pH units lower than the bulk pH (see Figure S2). This effect is strongly affected by the ionic strength of the medium. ASCn systems appear as formed mainly by neutral molecules when suspended in pure water, even at pH 5, which is > $pK_a$ [46]. Therefore, further studies of ASCn coagel thermal behaviour in relation to the pH are relevant in the context of their potential use as drug carriers.

Living human skin is maintained at an average temperature of 32 °C. If ASCn coagels are used for the topical application of AmB, this formulation should be efficient at this temperature. For systemic applications,

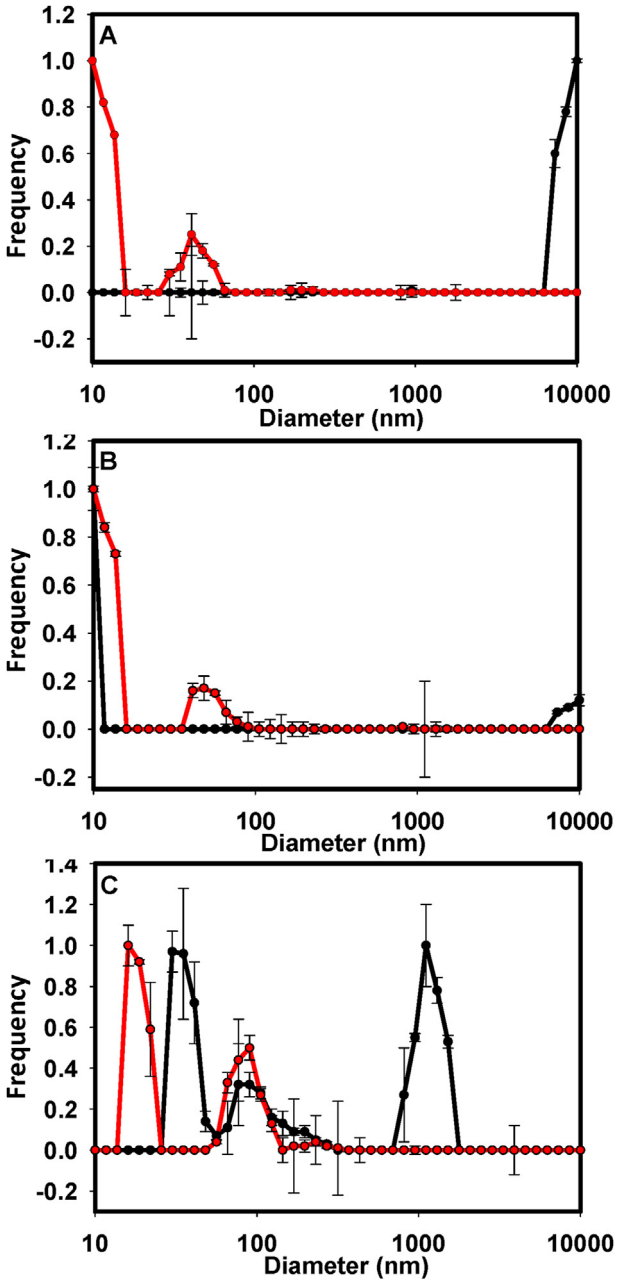


**Figure 6.** Analysis of the particle size distribution by DLS of aqueous suspensions of ASCn/AmB (20.4 μM AmB) at pH 4 (black lines) or pH 8 (red lines). The histograms correspond to ASC16 (A), ASC14 (B) or ASC12 (C). The analysis was performed considering the frequency of the particle's volume. The data corresponds to the average value from three independent experiments and the error bars correspond to SD.

the properties of formulations at 37 °C are relevant. Therefore, we explored whether the coagel structures studied in this work maintain their phase state at 22–25 °C (shelf temperature), and 32 °C. We performed differential scanning calorimetry (DSC) measurements of the ASC16 coagels at pH 8 and of the ASC12 coagels at pH 4 (Figure 7).

Our results show a sharp endothermic peak of ASC16 at pH 8, centred at (48.59 ± 0.06)°C, which shows an enthalpy change (ΔH) of (8.98 ± 0.4) kcal.mol$^{-1}$ (Figure 7A and Table S2). This value shifts to (47.84 ± 0.01) °C lowering the ΔH involved in this transition after five successive temperature scans. This transition process is associated with the endothermic transition of the acyl chains from an all-trans to trans/gauche isomerisation, similar to the thermal behaviour of lipids organised in

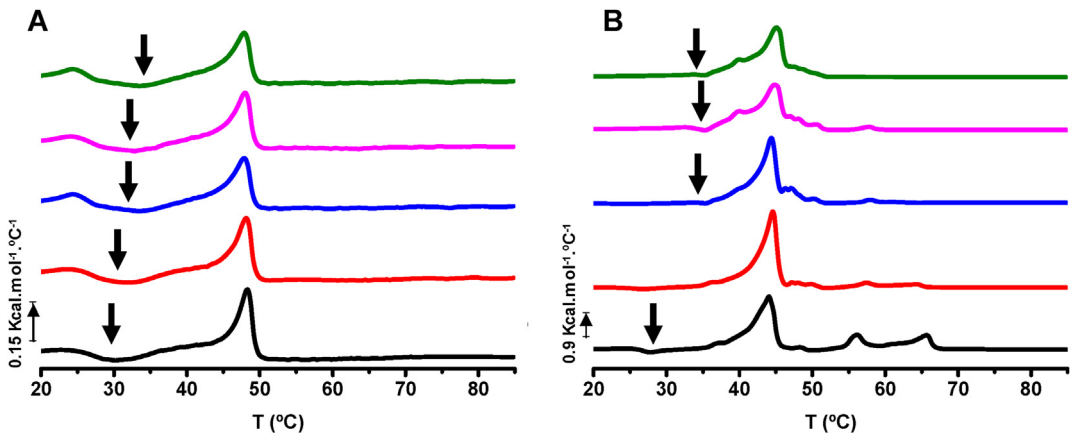


**Figure 7.** DSC of ASC16 pH 8 (A) and ASC12 pH 4 (B) coagels (2%w/v). The thermograms corresponding to the first (black), second (red), third (blue), fourth (magenta) and fifth scans (green) are plotted for both samples. The arrows indicate the exothermic peaks. The curves are the average of two independent experiments.

lamellas [58], and therefore, will be called melting temperature ($T_m$). The $T_m$ and ΔH values found are nearly 16 °C and 6 kcal $mol^{-1}$ lower than those observed for ASC16 coagels formed in pure water (63.8 °C) [32]. This clearly indicates that the self-organised structure formed by ASC16 at pH8 differs notably from that formed in pure water, probably due to the preponderance of the anionic form of the molecule in the former and the neutral in the latter condition.

A less-pronounced endothermic peak ($T_{endot\_1}$) with ΔH of (1.6 ± 0.1) kcal.$mol^{-1}$ was observed at (21.01 ± 0.04)°C, which increases in importance (and ΔH), shifting to (25.69 ± 0.05) °C after successive scans (see Figure 7A and Table S1). The occurrence of this peak roughly agrees with the reported phase transition for ascorbyl palmitate sodium salt aqueous suspension at 26 °C [57], supporting the predominance of the ionised form of ASC16.

Additionally, the thermograms of ASC16 coagels showed a broad exothermic peak ($T_{exot}$) with an ΔH (-0.08 ± 0.02) kcal.$mol^{-1}$ at (29.44 ± 0.01) °C that shifts to (34.5 ± 0.1) °C with successive scans (see Table S2 and arrows in Figure 7A). Similar behaviour has been reported by Blume [59] and by Kresheck [60] on DSC studies of ionic and non-ionic surfactants and appears to be a consequence of the temperature dependence of the CMC. These authors reported that the DSC curves exhibited a characteristic maximum at temperatures where the micellization or demicellization process occurs, and a minimum at the same temperature at which the CMC minimum is observed (in the 20–50 °C temperature range, depending on the nature of the surfactant). Therefore, both the endothermic peak observed for ASC16 coagels at 21–25 °C, as well as the exothermic peak at 29–35 °C, appear to be related to the micellization/demicellization process of ASC16.

It is also evident, from Figure 7A and the data in Table S2, that the ASC16 coagels underwent an annealing process along with the successive temperature scans, with the increasing importance of the low-temperature peaks enthalpy. It highlights a dominance of the micellization process in detriment of the main peak, which likely reflects the acyl chain structural transition in the lamellar aggregates. It is worth noticing that ASC16-diluted suspensions at pH8 show a significant population of small nanoparticles (micelles), as observed by DLS (Figure 6A). Our DSC results shown in Figure 7A suggest that ASC16 also forms an important proportion of micelles in the concentrated preparation (coagel).

ASC12 coagels at pH4 showed a strong endothermic peak (ΔH 33.6 ± 0.2 kcal $mol^{-1}$) at (45.22 ± 0.04) °C that shifts to (44.66 ± 0.05) °C after successive scans (Figure 7B and Table S1). This peak ($T_m$) probably reflects the melting of the acyl chains of the ASC12 molecules, in a similar way to that which occurs for lipids [58] and for ASC16 coagels. The $T_m$ for ASC12 coagels in acidic conditions is only 2–3 °C lower than the reported melting point for ASC12 coagels formed in pure water (47.3 °C) [32]. This suggests that, in both conditions, ASC12 is probably mainly present in its neutral form as a consequence of the ion double-layer effect and a low effective pH at the amphiphile/water surface [46].

Three smaller endothermic peaks, which together total an enthalpy value equivalent to a half of the main transition ΔH, were observed at higher temperatures (see Figure 7B and Table S2). These peaks appear and disappear and also shift their temperature along with the successive temperature scans, reducing the total ΔH to 2% of the main transition ΔH. This demonstrates a complex thermal behaviour, probably due to the coexistence of different aggregation forms of ASC12 that evolve to a more stable structure but suffer kinetic restrictions. It may also reflect the presence of poorly hydrated, crystalline forms of ASC12, which slowly hydrate with the temperature scanning process. DLS of a diluted suspension of ASC12 shows the presence of micro- and nanoparticles formed by ASC12 (Figure 6). These structures provide different environments for the ASC12 with very different curvatures of the interface plane. Thus, an annealing process may affect the dynamic equilibrium between these forms.

Similar to the ASC16 (pH 8) coagel explored above, ASC12 coagels (pH 4) show a broad, small exothermic peak (ΔH -1.65 ± 0.02 kcal $mol^{-1}$) at (27.83 ± 0.07)°C, which reduces its enthalpy with the successive scans. This suggests a small contribution of the micellization process to the overall thermal behaviour of the ASC12 preparation. This reflects a predominance of the compact and planar lamellas over the curved and more open micellar structures, probably as a consequence of the prevalence of the neutral form of the amphiphile.

### *3.4. Testing the capacity of ASCn monomolecular film to support monomeric AmB*

ASC16 coagels are formed by lamellar structures. Those are layered monomolecular films with a periodic organisation spaced 4.55 nm [33]. Here, we also explored the in-plane capacity of ASC16 and ASC12 films to disrupt or promote AmB aggregation by using Langmuir monolayers. This is a model system that represents the simplest unit block of the lamellar structure.

ASC16 films at the air/buffer solution (pH 8) interface organise as monomolecular films [46], which show the occurrence of a liquid-expanded to liquid-condensed phase transition at surface pressures >20 mN/m (Figure 8A and S2B). On the other hand, ASC16 films formed at pH 4 show the presence of two-dimensional crystals with in-plane optical anisotropy as observed by Brewster angle microscopy (BAM) (see Figure S2C and Ref. [46]).

When AmB is placed onto the air/water interface, it accommodates forming crystals that appear as optically anisotropic by BAM [61]. This behaviour was also observed in our ionic conditions (buffer solutions at pH 8 and 4, see Figure S6). Upon film compression, these crystalline

structures reorganise forming a thicker film with very high reflectivity. It is worth noting that the reflectivity signal of the BAM images is proportional to the thickness of the film [47,62].

AmB has been reported to have a hydrodynamic radius of 2.55 nm [63]. A film with such thickness would show reflectivity values of (5–6) x $10^{-6}$, depending on the assumed refraction index of the film (see Experimental Section). The average reflectivity observed for AmB films at high surface pressures exceeds 3 to 4-fold those values (not shown), evidencing the occurrence of aggregated forms of AmB that protrude from the film plane [61]. The compression isotherm of AmB films at the air/saline buffer pH8 shows a marked plateau at 10–15 mN/m (see Figure S7). This behavior agrees with previous reports performed using pure water as a subphase [49,61]. In those works, a compression-induced reorientation from the horizontal to the vertical position and further dimerization of AmB molecules are proposed to occur.

The incorporation of AmB into ASC16 films (pH 8) at increasing content of AmB (ASCn/AmB ratios from 8 to 1.25 w/w) induces a 2.5 increase in the reflectivity values, keeping the homogeneous appearance of the films (Figure 8A). The average reflectivity of those films is shown in Figure 8. Note that the values reached for ASC16/AmB films (pH 8) falls below the expected reflectivity for a film with a thickness of 2.55 nm, the length of an AmB molecule in aqueous environment [63]. In films containing ASCn/AmB at a ratio of 20 (w/w), the images were similar to that for 8 (w/w) (not shown).

Compression isotherms of ASC16/AmB at the air/saline buffer pH8 show that the reorientation evidenced by the curve plateau, shifts to higher surface pressures with a film enrichment in ASC16 (Figure S7), stabilizing the low surface pressure conformation of AmB [49]. Further analysis of the mean molecular area of ASC16/AmB mixed films indicates that AmB remains at the air/buffer interface, showing area expansion (Figure S7). This indicates that AmB molecules occupy larger areas when inserted into the ASC16 film in comparison with pure AmB films. This

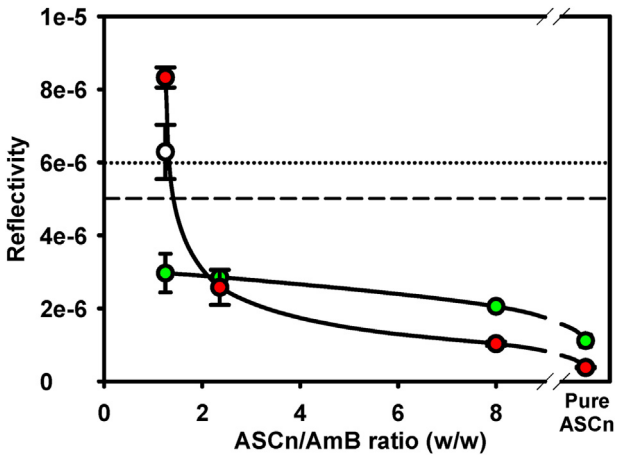


**Figure 9.** Reflectivity analysis of binary ASCn/AmB films. The average reflectivity calculated from BAM images of ASC16/AmB films at pH 8 (green) and ASC12/AmB films at pH 4 (red) at 20 mN/m was plotted as a function of the AmB content. As a comparison, the reflectivity of ASC16/AmB 1.25 w/w at pH 4 is also shown (white). Error bars reflect the standard deviation from two independent experiments. The horizontal lines indicate the reflectivity corresponding to a film with a thickness of 2.55 nm, calculated after Eq. (2) and considering the film refractive index $n = 1.433$ (dashed line) or 1.440 (dotted line).

behaviour evidenced a high capacity of ASC16 films for solubilising AmB molecules and agrees with the spectroscopy data that showed the prevalence of AmB in its monomeric form when inserted in ASC16 nanostructures at pH 8 (see Figures 1B and 3A).

Highly reflective structures were observed for ASC16/AmB films on buffer solution at pH 4 (Figure 8A, right panel and white symbol in

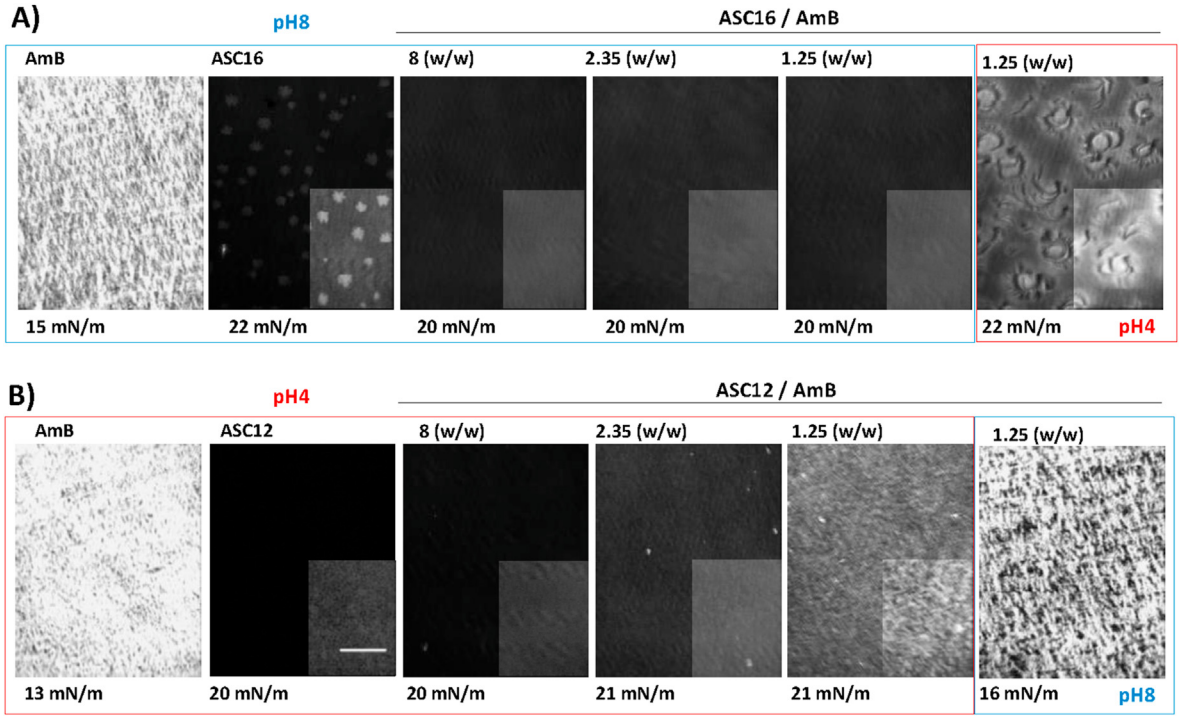


**Figure 8.** Brewster angle microscopy (BAM) visualisation of ASCn/AmB binary Langmuir films. A) Images of AmB or ASC16 monolayers at the air/buffer pH 8 interface and binary mixtures of both components containing an ASCn/AmB ratio of 8.00, 2.35° 1.25 (w/w) are shown. As a control, ASC16/AmB (1.25 w/w) is also shown when formed onto a buffer solution at pH 4. B) BAM images of AmB, ASC12 monolayers and binary mixtures of both components containing an ASCn/AmB ratio of 8, 2.35° 1.25 (w/w) at the air/buffer pH 4 interface. As a control, ASC12/AmB (1.25 w/w) is also shown when formed onto a buffer solution at pH 8. The background (bare air/water surface images) was subtracted from each BAM image. The grey level reflects the original relation to the film thickness and refractive index as detailed in Section 2.5. For better visualization of surface texture, contrast-enhanced images are shown as insets. The surface pressures are indicated for each image. The images are representative of two independent experiments. Scale bar is 50 μm.

Figure 9), a condition that evidenced the presence of AmB aggregates by spectroscopy. The curious in-plane structure observed in this sample (shown in detail in Figure S8) appears as a consequence of a first phase transition of ASC16 upon film compression, similar to that observed previously for pure ASC16 films [34,46]. This event is followed by the crystallisation of AmB, which forms thick structures that nucleate at the previously formed domain interface.

We tested Langmuir films formed by ASC12/AmB onto buffer solution at pH 4 (Figure 8B). This composition and ionic condition show signs of AmB oligomerization/aggregation by spectroscopy studies (Figures 1D and 3B). Those films show a hyperbolic-like increase of the average reflectivity, which increases 22-fold the value of the control ASC12 films in the absence of AmB and reaches values higher than expected for a film with a thickness of 2.55 nm (see horizontal lines in Figure 9). This effect is even larger at pH 8, showing a thick crystalline structure (Figure 8B, right panel), evidencing the limited capacity of ASC12 films to laterally solubilise AmB molecules. Previous reports indicate that the monomeric form of AmB has stronger affinities to lipid bilayers than the dimeric/aggregated forms [20]. The results shown in this section suggest parallelism for the AmB behaviour when incorporated into ASCn films and phospholipid bilayers.

## 4. Discussion

In the present study we tested the hypothesis that a formulation capable of maintaining AmB in the monomeric form will result in a more efficient antimicrobial than those that show oligomerization signs by UV-visible spectroscopy analysis. Our results indicate that this is not the case when two similar formulations are compared. However, the evidences of a better antimicrobial performance of monomeric AmB loaded suspensions accumulated in literature may be more related to its chemical and colloidal stability than to its effect against the yeast cells.

Our study highlights the capacity of nanostructures formed by ASC16 in its anionic form for providing an appropriate environment to support the monomeric form of AmB, which preserves its chemical and structural stability as well as its antimicrobial activity for long periods. This formulation constitutes an aqueous-based (organic solvent-free) nanostructure, which appears as appealing for further tests for the treatment of cutaneous infections. The UV-visible and CD absorption spectroscopy studies indicated a predominance of the monomeric form of AmB, which has also been reported for other micellar-based formulations [25,26,30]. In this work, we relate ASC16 coagels capacity for maintaining the in-plane solubility of AmB, which may be responsible for its enhanced chemical stability. The ascorbic moiety of the ASC16 provides an antioxidant environment that would add to the chemical stability of AmB. In addition, the physicochemical analysis of the ASC16/AmB systems formed at neutral pH indicates that those preparations show mainly nanometric-sized structures with very negative zeta potential values, which is important for maintaining the stability of the colloidal system. The technological advantages of the nanoformulation presented here are the easy and low-cost synthesis of the ASCn compounds [34] as well as the technically simple assembly of the nanostructures. On the contrary, ASC12 coagels, besides maintaining the antimicrobial capacity of AmB, show poor ability to solubilise AmB in the lamellar plane of the nanostructures. This agrees with the spectroscopic evidence of AmB aggregation. AmB molecules may be expelled to the interllamelar spaces and exposed to the aqueous acidic environment, contributing to the chemical instability observed in a period of days. Furthermore, the large size of the ASC12 self-assembled structures and its low negative zeta potential led to structural heterogeneity and colloidal instabilityASC16/AmB formulations at pH8, self-organise in nanostructures with a negative surface charge that remains in a phase state similar to the lipid gel phase during the range of temperature relevant for topic treatment. The results also show strong evidence of coexistence between a lamellar and a micellar phase. In the context of the mechanism of enhanced skin permeation, the presence of ASC16-based micelles may work as the mobile fraction of the formulation, which easily interacts with the stratum corneum of the skin, whilst the larger lamellar structures might remain as a reservoir for providing a long-term release of ASC16/AmB micelles.

In our recent work [64], we demonstrated that ASC16 interacts with lipids that compounds the stratum corneum of the skin. ASCn relax the stiffness of this tight lipid layer, increasing its elasticity. In the nanometer scale, ASCn also alter the membrane heterogeneity, enlarging the cholesterol-enriched phase and reducing the more rigid ceramide-enriched phase. The overall effect contributes to a partition-diffusion process through the stratum corneum multiple layers. Our hypothesis is based on that the alteration of the physical properties of the stratum corneum induced by ASC16 will promote the incorporation of AmB and favours its diffusion to reach the drug target.

It has been reported that AmB organises parallel to the surface of Polysorbate 80 micelles [63], which is important for the AmB solubilisation power of the detergent suspension. However, if this were the case for all the ASCn structures tested, AmB would be equally solubilised in the monomeric form for all ASCn nanostructures (in similar ionic conditions).

Spectroscopic studies combined with molecular simulations showed that the basic constituent of the AmB aggregated structure is a tetramer composed of two hydrogen-bond-stabilised dimers, each dimer formed by molecules interacting antiparallel relative to each other [14,20]. AmB is proposed to have a length of 2.55 nm for the monomer [63], and 3.2 nm for the antiparallel dimer (J-aggregates) [20]. Therefore, the thickness of the hydrophobic portion of the ASCn structure that supports AmB may act as a regulation point for the equilibrium between the dimer and monomer forms (Scheme 2).

ASC16 aqueous suspensions form 4.55 nm thick lamellae, as studied by x-ray diffraction [33]. Therefore, it can easily accommodate an AmB molecule (2.55 nm length) in each hemilayer. In this way, the thicker lamellas formed by ASC16 may truly solubilise AmB molecules into the hydrophobic core of the membrane, keeping the charged groups (amine and carboxylic) near the polar ascorbic group, similar to the conformation proposed when arranged in sterol-containing membranes [12].

A simple calculation based on the acyl chain length [65] estimates that the ASC14 and ASC12 lamellas may be 0.52 and 1.04 nm thinner (4.03 nm for ASC14, and 3.51 nm for ASC12 bilayers), respectively. Thin lamellar structures formed by ASC12 may not be able to support AmB molecules independently in both hemilayers. However, it may favour the occurrence of antiparallel AmB dimer, whose dimensions (3.2 nm) are close to the bilayer thickness formed by ASC12 (3.51 nm) (see Scheme 2). Furthermore, AmB molecules inserted in the ASC12 film may undergo lateral segregation from the surrounding film as a consequence of hydrophobic mismatch, which would favour AmB aggregation. Lateral segregation driven by hydrophobic mismatch has been extensively reported for membrane proteins immersed in lipid bilayers of different thicknesses [66] as well as for explaining lipid domain segregation [67]. .

Langmuir film visualisation supports spectrophotometric evidence that anionic ASC16 allows the in-plane solubilisation of AmB. This is not the case for ASC12 films or ASC16 films in acidic conditions, where the observation of thick structures evidenced the occurrence of AmB aggregates. The anionic form of ASC16 induced a more relaxed film structure in comparison with the neutral ASC16, which form liquid-condensed phases [46]. Previous work of our group on drug-lipid membrane interactions highlights the relevance of the phase state and rheological properties of the host membrane in its capacity to incorporate amphiphilic drugs. Thus, an increase in rigidity of the film (an increase of the compressibility modulus) was found to correlate with lower drug incorporation [68,69].

ASCn self-organises into lamellar arrangements that closely resemble lipid membranes [33,34,46]. Here, we found that the ionisation state of ASC16 aggregates regulates the incorporation into the hydrophobic layer of the lamella of AmB molecules in the ASC16/AmB system. This agrees with our previous experience since anionic ASC16 form films with lower rigidity properties than when formed by neutral molecules [34]. This

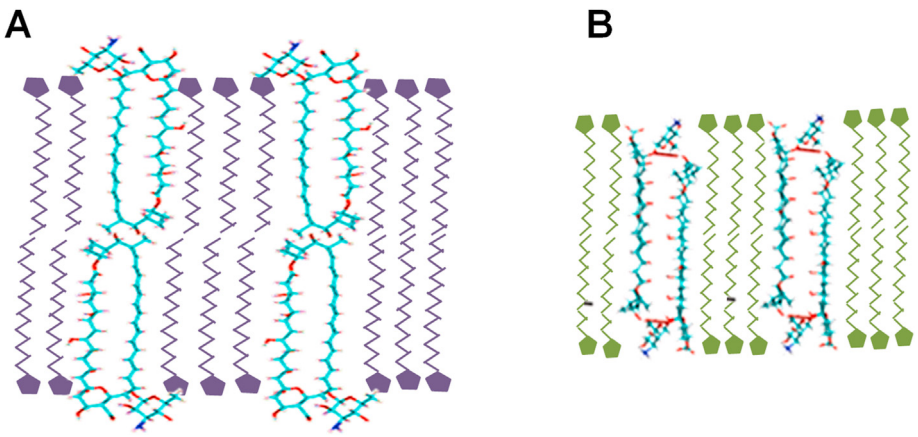


**Scheme 2.** Graphical representation of the conformation proposed for AmB when inserted into ASC16 (A) or ASC12 (B) lamellas. AmB structures in a monomeric (A) or dimer (B) conformation were adapted from Ref. [20].

effect may also be favoured by a strong electrostatic interaction between the anionic ascorbyl group and the charged AmB groups, stabilising insertion at the polar group layer.

A recent report provides evidence that Nystatin, another polyene antimycotic structurally close related to AmB incorporates favourably within phospholipid-enriched gel domains, with some differences for phosphatidylcholine and sphingomyelin gel phases [70]. Those gel phases may show differences in membrane thickness as well as other physical properties. DSC results show that ASC16 form self-aggregated structures with thermotropic behaviour that resembles the gel phase of lipid membranes. In this context, our results agree with the observed for Nystatin, since AmB appears to be stably incorporated into the gel-like phase of ASC16 and being very sensitive to the thickness of the lamellar structure.

Finally, ASC16 coagels as well as ASC14 and ASC12 have been proposed as good skin permeation enhancers [41]. ASC16 is also currently used in a large spectrum of cosmetic products and proposed in a variety of drug delivery systems, showing mild irritation effects [35,71,72]. Our DSC results indicate that ASC16 coagels formed at neutral pH underwent their main transitions at 47–48 °C, well above the storage and therapeutic temperature (32 °C). This suggests that the AmB incorporated into the lamellar sheets interact with the acyl chains of ASC16 in the same phase state in this temperature range. This result suggests that the coagels act probably as a reservoir of the drug that could be useful when longer delivery times are required.

Therefore, the positive properties of ASC16 formulations as a drug carrier for dermal delivery [32,40], together with the results shown in the present work, make this nanostructured system appealing for further tests for the treatment of cutaneous mycotic and parasitic infections. Among these, cutaneous *Leishmaniasis* is the desired target for such pharmaceutical development, in particular in endemic countries such as Brazil and Argentina [4]. The achievement of an effective topical treatment for cutaneous parasitic and mycotic infection would prevent the systemic use of AmB, lowering the overall toxic effect of this drug.

## Declarations

### *Author contribution statement*

Maria Laura Fanani, Raquel V Vico: Conceived and designed the experiments; Analyzed and interpreted the data; Contributed reagents, materials, analysis tools or data; Wrote the paper.

Natalia E Nocelli: Performed the experiments; Analyzed and interpreted the data; Wrote the paper.

Yenisleidy M Zulueta Díaz: Contributed reagents, materials, analysis tools or data; Wrote the paper.

Marine Millot, Maria Luz Colazo: Performed the experiments.

### *Funding statement*

Natalia E Nocelli was supported by Consejo Nacional de Investigaciones Científicas y Técnicas (CONICET), Argentina (Beca Posdoc). Maria Laura Fanani and Raquel V. Vico are Career Investigators of CONICET. Maria Laura Fanani was supported by Fondo para la Investigación Científica y Tecnológica (PICT 2017-0332). Raquel V Vico was supported by Fondo para la Investigación Científica y Tecnológica (PICT 2016-0262). Maria Laura Fanani was supported by Secretaria de Ciencia y Tecnología - Universidad Nacional de Córdoba (SECyT-UNC), Argentina.

### *Data availability statement*

Data included in article/supplementary material/referenced in article.

### *Declaration of interests statement*

The authors declare no conflict of interest.

### *Additional information*

Supplementary content related to this article has been published online at https://doi.org/10.1016/j.heliyon.2021.e06056.

## Acknowledgements

We thank Dr. Javier Valdez Taubas for the generous gift of the yeast strain *Saccharomyces cerevisiae* BY4741, ATCC 201388. The BAM experiments were performed at the “Centro de Micro y Nanoscopía de Córdoba” (CEMINCO-CIQUIBIC) working as part of the “Sistema Nacional de Microscopía (SNM)”. The authors thank Dr. Soledad Bazán (CPA career-CONICET) for technical assistance in particle analysis and DSC experiments and Dr. Matias Crosio for useful discussions.

## References

[1] G.M. Soliman, Nanoparticles as safe and effective delivery systems of antifungal agents: achievements and challenges, Int. J. Pharm. 523 (2017) 15–32.
[2] J.J. Torrado, R. Espada, M.P. Ballesteros, S. Torrado-Santiago, Amphotericin B formulations and drug targeting, J. Pharmacol. Sci. 97 (2008) 2405–2425.
[3] V. Yardley, S.L. Croft, A comparison of the activities of three amphotericin B lipid formulations against experimental visceral and cutaneous leishmaniasis, Int. J. Antimicrob. Agents 13 (2000) 243–248.

[4] R. Reithinger, J. Dujardin, H. Louzir, Cutaneous leishmaniasis, Lancet Infect. Dis. 7 (2007) 581–596.
[5] C. Stritzler, Cutaneous candidiasis treated with topical amphotericin B, Arch. Dermatol. 93 (1966) 101.
[6] E. Evans, What interventions are effective for the prevention and treatment of cutaneous candidiasis? J. WOCN. 30 (2003) 11–16.
[7] A. Manosroi, L. Kongkaneramit, J. Manosroi, Stability and transdermal absorption of topical amphotericin B liposome formulations, Int. J. Pharm. 270 (2004) 279–286.
[8] A. Hussain, A. Samad, S.K. Singh, M.N. Ahsan, A. Faruk, F.J. Ahmed, Enhanced stability and permeation potential of nanoemulsion containing sefsol-218 oil for topical delivery of amphotericin B, Drug Dev. Ind. Pharm. 41 (2015) 780–790.
[9] M.F. Peralta, M.L. Guzmán, A.P. Pérez, G.A. Apezteguia, M.L. Fórmica, E.L. Romero, M.E. Olivera, D.C. Carrer, Liposomes can both enhance or reduce drugs penetration through the skin, Sci. Rep. 8 (2018) 1–11.
[10] S. Trombino, S. Mellace, R. Cassano, Solid lipid nanoparticles for antifungal drugs delivery for topical applications, Ther. Deliv. 7 (2016) 639–647.
[11] C. López-Castillo, C. Rodríguez-Fernández, M. Córdoba, J.J. Torrado, Permeability characteristics of a new antifungal topical amphotericin B formulation with γ-cyclodextrins, Molecules (2018).
[12] A. Chattopadhyay, M. Jafurulla, A novel mechanism for an old drug: amphotericin B in the treatment of visceral leishmaniasis, Biochem. Biophys. Res. Commun. 416 (2011) 7–12.
[13] E. Grela, M. Wieczór, R. Luchowski, J. Zielinska, A. Barzycka, W. Grudzinski, K. Nowak, P. Tarkowski, J. Czub, W.I. Gruszecki, Mechanism of binding of antifungal antibiotic amphotericin B to lipid membranes: an insight from combined single-membrane imaging, microspectroscopy, and molecular dynamics, Mol. Pharm. 15 (2018) 4202–4213.
[14] J. Starzyk, M. Gruszecki, K. Tutaj, R. Luchowski, R. Szlazak, P. Wasko, W. Grudzinski, J. Czub, W.I. Gruszecki, Self-association of amphotericin b: spontaneous formation of molecular structures responsible for the toxic side effects of the antibiotic, J. Phys. Chem. B 118 (2014) 13821–13832.
[15] H.E. Lambing, B.D. Wolf, S.C. Hartsel, Temperature effects on the aggregation state and activity of Amphotericin B, BBA - Biomembr 1152 (1993) 185–188.
[16] P. Legrand, E.A. Romero, B.E. Cohen, J. Bolard, Effects of aggregation and solvent on the toxicity of amphotericin B to human erythrocytes, Antimicrob. Agents Chemother. 36 (1992) 2518–2522.
[17] J. Bolard, P. Legrand, F. Heitz, B. Cybulska, One-sided action of amphotericin B on cholesterol-containing membranes is determined by its self-association in the medium, Biochemistry 30 (1991) 5707–5715.
[18] J. Barwicz, S. Christian, I. Gruda, Effects of the aggregation state of amphotericin B on its toxicity to mice, Antimicrob. Agents Chemother. 36 (1992) 2310–2315.
[19] M.L. Adams, G.S. Kwon, Relative aggregation state and hemolytic activity of amphotericin B encapsulated by poly(ethylene oxide)-block-poly(N-hexyl-L-aspartamide)-acyl conjugate micelles: effects of acyl chain length, J. Contr. Release 87 (2003) 23–32.
[20] P. Wasko, R. Luchowski, K. Tutaj, W. Grudzinski, P. Adamkiewicz, W.I. Gruszecki, Toward understanding of toxic side effects of a polyene antibiotic amphotericin B: fluorescence spectroscopy reveals widespread formation of the specific supramolecular structures of the drug, Mol. Pharm. 9 (2012) 1511–1520.
[21] J. Barwicz, M. Beauregard, P. Tancrède, Circular dichroism study of interactions of Fungizone or AmBisome forms of amphotericin B with human low density lipoproteins, Biopolym. - Biospectroscopy Sect. 67 (2002) 49–55.
[22] Q. Zia, O. Mohammad, M.A. Rauf, W. Khan, S. Zubair, Biomimetically engineered Amphotericin B nano-aggregates circumvent toxicity constraints and treat systemic fungal infection in experimental animals, Sci. Rep. 7 (2017).
[23] M.D. Moen, K.A. Lyseng-Williamson, L.J. Scott, Liposomal Amphotericin B, Drugs, 2009, pp. 361–392, 69.
[24] F. Gaboriau, M. Chéron, C. Petit, J. Bolard, Heat-induced superaggregation of amphotericin B reduces its in vitro toxicity: a new way to improve its therapeutic index, Antimicrob. Agents Chemother. 41 (1997) 2345–2351.
[25] V. Leonhard, R. Alasino, I. Bianco, A. Garro, V. Heredia, D. Beltramo, Biochemical characterization of GM1 micelles-amphotericin B interaction, Curr. Drug Deliv. 12 (2015) 406–414.
[26] A.H.A. Mohamed-Ahmed, K.A. Les, S.L. Croft, S. Brocchini, Preparation and characterisation of amphotericin B-copolymer complex for the treatment of leishmaniasis, Polym. Chem. 4 (2013) 584–591.
[27] G. Vandermeulen, L. Rouxhet, A. Arien, M.E. Brewster, V. Préat, Encapsulation of amphotericin B in poly(ethylene glycol)-block-poly(ε- caprolactone-co-trimethylenecarbonate) polymeric micelles, Int. J. Pharm. 309 (2006) 234–240.
[28] P. Jansook, W. Pichayakorn, G.C. Ritthidej, Amphotericin B-loaded solid lipid nanoparticles (SLNs) and nanostructured lipid carrier (NLCs): effect of drug loading and biopharmaceutical characterizations, Drug Dev. Ind. Pharm. 44 (2018) 1693–1700.
[29] P. Jansook, Z. Fülöp, G.C. Ritthidej, Amphotericin B loaded solid lipid nanoparticles (SLNs) and nanostructured lipid carrier (NLCs): physicochemical and solid-solution state characterizations, Drug Dev. Ind. Pharm. 45 (2019) 560–567.
[30] G. Vandermeulen, L. Rouxhet, A. Arien, M.E. Brewster, V. Préat, Encapsulation of amphotericin B in poly(ethylene glycol)-block-poly(ϵ-caprolactone-co-trimethylenecarbonate) polymeric micelles, Int. J. Pharm. 309 (2006) 234–240.
[31] S. Palma, R.H. Manzo, D. Allemandi, L. Fratoni, P. Lo Nostro, Coagels from ascorbic acid derivatives, Langmuir 18 (2002) 9219–9224.
[32] S. Palma, R. Manzo, P. Lo Nostro, D. Allemandi, Nanostructures from alkyl vitamin C derivatives (ASCn): properties and potential platform for drug delivery, Int. J. Pharm. 345 (2007) 26–34.
[33] M. Mottola, N. Wilke, L. Benedini, R.G. Oliveira, M.L. Fanani, Ascorbyl palmitate interaction with phospholipid monolayers: electrostatic and rheological preponderancy, Biochim. Biophys. Acta Biomembr. 1828 (2013) 2496–2505.
[34] M. Mottola, R.V. Vico, M.E. Villanueva, M.L. Fanani, Alkyl esters of l-ascorbic acid: stability, surface behaviour and interaction with phospholipid monolayers, J. Colloid Interface Sci. 457 (2015) 232–242.
[35] L.I. Tártara, D.A. Quinteros, V. Saino, D.A. Allemandi, S.D. Palma, Improvement of acetazolamide ocular permeation using ascorbyl laurate nanostructures as drug delivery system, J. Ocul. Pharmacol. Therapeut. 28 (2012).
[36] V. Saino, D. Monti, S. Burgalassi, S. Tampucci, S. Palma, D. Allemandi, P. Chetoni, Optimization of skin permeation and distribution of ibuprofen by using nanostructures (coagels) based on alkyl vitamin C derivatives, Eur. J. Pharm. Biopharm. 76 (2010) 443–449.
[37] K. Moribe, S. Maruyama, Y. Inoue, T. Suzuki, T. Fukami, K. Tomono, K. Higashi, Y. Tozuka, K. Yamamoto, Ascorbyl dipalmitate/PEG-lipid nanoparticles as a novel carrier for hydrophobic drugs, Int. J. Pharm. 387 (2010) 236–243.
[38] M.F. Sánchez Vallecillo, G.V. Ullio Gamboa, S.D. Palma, M.F. Harman, A.L. Chiodetti, G. Morón, D.A. Allemandi, M.C. Pistoresi-Palencia, B.A. Maletto, Adjuvant activity of CpG-ODN formulated as a liquid crystal, Biomaterials 35 (2014) 2529–2542.
[39] L. Benedini, S. Antollini, M.L. Fanani, S. Palma, P. Messina, P. Schulz, Study of the influence of ascorbyl palmitate and amiodarone in the stability of unilamellar liposomes, Mol. Membr. Biol. 31 (2014).
[40] S.D. Palma, G.V. Ullio Gamboa, D.A. Allemandi, Vitamin C based nanostructures: potential utility in ocular and transdermal therapy, J. Biomater. Tissue Eng. 3 (2013) 61–69.
[41] S.D. Palma, B. Maletto, P. Lo Nostro, R.H. Manzo, M.C. Pistoresi-Palencia, D.A. Allemandi, Potential use of ascorbic acid-based surfactants as skin penetration enhancers, Drug Dev. Ind. Pharm. 32 (2006) 821–827.
[42] M.L. Fanani, R.V. Vico, L. Benedini, Alkyl Esters of L-Ascorbic Acid: from Synthesis to Applications, 2017.
[43] J.L. Rios, M.C. Recio, A. Villar, Screening methods for natural products with antimicrobial activity: a review of the literature, J. Ethnopharmacol. 23 (1988) 127–149.
[44] C.B. Brachmann, A. Davies, G.J. Cost, E. Caputo, J. Li, P. Hieter, J.D. Boeke, Designer deletion strains derived from Saccharomyces cerevisiae S288C: a useful set of strains and plasmids for PCR-mediated gene disruption and other applications, Yeast 14 (1998) 115–132.
[45] P. Somasegaran, H.J. Hoben, Handbook for rhizobia, in: Methods Legum. Technol., Springer-Verlag Inc., 1994.
[46] L. Benedini, M.L. Fanani, B. Maggio, N. Wilke, P. Messina, S. Palma, P. Schulz, Surface phase behavior and domain topography of ascorbyl palmitate monolayers, Langmuir 27 (2011).
[47] D. Vollhardt, Brewster angle microscopy: a preferential method for mesoscopic characterization of monolayers at the air/water interface, Curr. Opin. Colloid Interface Sci. 19 (2014) 183–197.
[48] D. Ducharme, J. Max, C. Salesse, R.M. Leblanc, Ellipsometric study of the physical states of phosphatidylcholines at the air-water interface, J. Phys. Chem. 94 (1990) 1925–1932.
[49] M. Gagos, I. Gruszecki, Organization of polyene antibiotic amphotericin B at the argon – water interface, Biophys. Chem. 137 (2008) 110–115.
[50] M. Gagoś, M. Arczewska, Spectroscopic studies of molecular organization of antibiotic amphotericin B in monolayers and dipalmitoylphosphatidylcholine lipid multibilayers, Biochim. Biophys. Acta Biomembr. 1798 (2010) 2124–2130.
[51] M. Gagoś, M. Hereć, M. Arczewska, G. Czernel, M. Dalla Serra, W.I. Gruszecki, Anomalously high aggregation level of the polyene antibiotic amphotericin B in acidic medium: implications for the biological action, Biophys. Chem. 136 (2008) 44–49.
[52] K. Gilani, E. Moazeni, T. Ramezanli, M. Amini, M.R. Fazeli, H. Jamalifar, Development of respirable nanomicelle carriers for delivery of amphotericin B by jet nebulization, J. Pharmacol. Sci. 100 (2011) 252–259.
[53] L.P. Jameson, S.V. Dzyuba, Circular dichroism studies on intermolecular interactions of amphotericin B in ionic liquid-rich environments, Chirality 25 (2013) 427–432.
[54] F. Gaboriau, M. Chéron, L. Leroy, J. Bolard, Physico-chemical properties of the heat-induced "superaggregates" of amphotericin B, Biophys. Chem. 66 (1997) 1–12.
[55] M. Gagoś, G. Czernel, Oxidized forms of polyene antibiotic amphotericin B, Chem. Phys. Lett. 598 (2014) 5–9.
[56] G. Czernel, R. Typek, K. Klimek, A. Czuryło, A.L. Dawidowicz, M. Gagoś, Catalytic effect of free iron ions and heme-iron on chromophore oxidation of a polyene antibiotic amphotericin B, J. Mol. Struct. 1111 (2016) 69–75.
[57] S. Palma, P. Lo Nostro, R. Manzo, D. Allemandi, Evaluation of the surfactant properties of ascorbyl palmitate sodium salt, Eur. J. Pharmaceut. Sci. 16 (2002) 37–43.
[58] T. Heimburg, Thermal Biophysics of Membranes, WILEY-VCH Verlag GmbH & Co. KGaA, Germany, 2007.
[59] P.R. Majhi, A. Blume, Thermodynamic characterization of temperature-induced micellization and demicellization of detergents studied by differential scanning calorimetry, Langmuir 17 (2001) 3844–3851.
[60] G.C. Kresheck, Interpretation of the differential scanning calorimetry curves for aqueous solutions of three nonionic surfactants, Langmuir 16 (2000) 3067–3069.
[61] J. Miñones, C. Carrera, P. Dynarowicz Latka, J. Miñones, O. Conde, R. Seoane, J.M. Rodríguez Patino, Orientational changes of amphotericin B in Langmuir monolayers observed by Brewster angle microscopy, Langmuir 17 (2001) 1477–1482.

[62] C. Lheveder, J. Meunier, S. Henon, Brewster angle microscopy, in: A. Baszkin, W. Norde (Eds.), Phys. Chem. Biol. Interfaces, first ed., Marcel Dekker, Inc., NEW YORK BASEL, 2000.
[63] M. Mobasheri, H. Attar, S.M.R. Sorkhabadi, A. Khamesipour, M.R. Jaafari, Solubilization behavior of polyene antibiotics in nanomicellar system: insights from molecular dynamics simulation of the amphotericin B and Nystatin interactions with polysorbate 80, Molecules (2016) 21.
[64] Y. de las M. Zulueta Díaz, K. Menghi, M.L. Guerrero, N. Nocelli, M.L. Fanani, l-Ascorbic acid alkyl esters action on stratum corneum model membranes: an insight into the mechanism for enhanced skin permeation, Colloids Surf. B Biointerfaces 185 (2020) 110621.
[65] D.A. Peñalva, G.M. Oresti, F. Dupuy, S.S. Antollini, B. Maggio, M.I. Aveldaño, M.L. Fanani, Atypical surface behavior of ceramides with nonhydroxy and 2-hydroxy very long-chain (C28-C32) PUFAs, Biochim. Biophys. Acta Biomembr. 1838 (2014).
[66] F. Dumas, M.C. Lebrun, J.F. Tocanne, Is the protein/lipid hydrophobic matching principle relevant to membrane organization and functions? FEBS Lett. 458 (1999) 271–277.
[67] E.J. Wallace, N.M. Hooper, P.D. Olmsted, Effect of hydrophobic mismatch on phase behavior of lipid membranes, Biophys. J. 90 (2006) 4104–4118.
[68] Y. de las M. Zulueta Díaz, M. Mottola, R.V. Vico, N. Wilke, M.L. Fanani, The rheological properties of lipid monolayers modulate the incorporation of L-ascorbic acid alkyl esters, Langmuir 32 (2016) 587–595.
[69] Y. de las M. Zulueta Díaz, M.L. Fanani, Crossregulation between the insertion of Hexadecylphosphocholine (miltefosine) into lipid membranes and their rheology and lateral structure, Biochim. Biophys. Acta Biomembr. 1859 (2017) 1891–1899.
[70] A.G. Dos Santos, J.T. Marquês, A.C. Carreira, I.R. Castro, A.S. Viana, M.P. Mingeot-Leclercq, R.F.M. De Almeida, L.C. Silva, The molecular mechanism of Nystatin action is dependent on the membrane biophysical properties and lipid composition, Phys. Chem. Chem. Phys. 19 (2017) 30078–30088.
[71] M. Üner, S.A. Wissing, G. Yener, R.H. Müller, Skin moisturizing effect and skin penetration of ascorbyl palmitate entrapped in Solid Lipid Nanoparticles (SLN) and Nanostructured Lipid Carriers (NLC) incorporated into hydrogel, Pharmazie 60 (2005) 751–755.
[72] M. Gosenca, M. Bešter-Rogač, M. Gašperlin, Lecithin based lamellar liquid crystals as a physiologically acceptable dermal delivery system for ascorbyl palmitate, Eur. J. Pharmaceut. Sci. 50 (2013) 114–122.